An Explicit Finite Element Method for Inviscid Compressible Flow

Wiroj Limtrakarn
Graduate Student

Pramote Dechaumphai
Professor

Mechanical Engineering Department, Chulalongkorn University
Bangkok 10330, Thailand

Abstract

An explicit finite element method for the two-dimensional inviscid compressible flow is presented. The finite element equations are derived and its computational procedure is described. The method is validated by developing a corresponding computer program that can be executed on standard personal computers. Several examples are presented to demonstrate the capability and accuracy of the proposed method.

1. Introduction

High-speed compressible flow past complex geometry normally includes several flow phenomena such as shock waves, expansion waves and shock-shock interactions [1,2]. Most of these flow features are characterized by steep gradients that need robust computational techniques for accurate solutions. In the past decade, several finite element algorithms have been developed. These algorithms include the Petrov-Galerkin algorithm [3], the least-squares algorithm [4], the upwind cell-centered algorithm [5], and the Taylor-Galerkin algorithm [6].

In this paper, the explicit two-step Taylor-Galerkin algorithm has been investigated because of its high accuracy and robustness in capturing complex flow behavior. The paper starts by explaining the theoretical formulation and the derivation of the finite element equations for inviscid compressible flow analysis that leads to the development of a corresponding computer program. This Taylor-Galerkin finite element algorithm is then evaluated by analyzing four problems of: a Mach 3 flow past a wedge; a Mach 2.6 flow in a channel with compression and expansion ramps; a Mach 6.57 flow past a cylinder; and a Mach 6.57 flow past two cylinders with shock-shock interaction phenomenon.

2. Theoretical Formulation

2.1 Governing Differential Equations

The Euler equations for inviscid laminar compressible flow are governed by the conservation of mass, momentums, and energy. These equations, in two dimensions, are written in the conservation form [7] as,

$$\frac{\partial}{\partial t}\{U\} + \frac{\partial}{\partial x}\{E\} + \frac{\partial}{\partial y}\{F\} = 0 \qquad (1)$$

The vector $\{U\}$ contains the conservation variables defined by,

$$\{U\} = \begin{Bmatrix} \rho \\ \rho u \\ \rho v \\ \rho \varepsilon \end{Bmatrix} \qquad (2)$$

where ρ is the fluid density; u and v are the velocity components in the x and y directions, respectively; and ε is the total energy. The $\{E\}$ and $\{F\}$ vectors consist of the inviscid fluxes in the x and y directions, respectively. These inviscid flux vectors are given by,

$$\{E\} = \begin{Bmatrix} \rho u \\ \rho u^2 + p \\ \rho uv \\ \rho u\varepsilon + pu \end{Bmatrix} \quad ; \quad \{F\} = \begin{Bmatrix} \rho v \\ \rho uv \\ \rho v^2 + p \\ \rho v\varepsilon + pv \end{Bmatrix} \qquad (3)$$

where p is the pressure. The total energy that consists of the internal energy and the kinetic energy is defined by,

$$\varepsilon = e + \frac{1}{2}\left(u^2 + v^2\right) \qquad (4)$$

where e is the internal energy that can be written in the form,

$$e = c_v T \qquad (5)$$

where c_v is the specific heat at constant volume, and T is the temperature.

2.2 Finite Element Formulation

The basic concept of the explicit two-step Taylor-Galerkin algorithm [8] is to use: 1) the Taylor series expansion in time to establish recurrence relations for time marching, and 2) the method of weighted residuals with Galerkin's criteria for spatial discretization for deriving the finite element equations.

The computation proceeds through two steps. At the first step, the conservation variable $\{U\}$ is assumed constant over the element and are computed explicitly. At the second step, these constant element quantities are then used to compute the nodal quantities. Details of such procedure are given below.

2.2.1) The first step

Using the first order Taylor series at time $t = t_{n+1/2}$ the conservation variable is written as,

$$U^{n+1/2} = U^n + \frac{1}{2}\Delta t \left.\frac{\partial U}{\partial t}\right|^n \tag{6}$$

where superscript n and n+1/2 denote the evaluation at time $t = t_n$ and $t = t_{n+1/2}$, respectively. Then Eq. (1) is substituted into the right-hand side of Eq. (6) so that,

$$U^{n+1/2} = U^n - \frac{\Delta t}{2}\left[\frac{\partial E}{\partial x}+\frac{\partial F}{\partial y}\right]^n \tag{7}$$

At time $t_{n+1/2}$, $U^{n+1/2}$ is assumed to be constant over element and at time t_n, the variable U^n, E^n and F^n are interpolated from the element nodal values as,

$$U^{n+1/2} = U_e^{n+1/2} \tag{8a}$$

$$U^n = \sum_j N_j U_j^n \tag{8b}$$

$$E^n = \sum_j N_j E_j^n \tag{8c}$$

$$F^n = \sum_j N_j F_j^n \tag{8d}$$

where N_j is the linear interpolation functions for the triangular element. The spatial approximation given in Eq. (8) are substituted into Eq. (7). The method of weighted residuals is then applied over the element area, Ω, to yield the element equations as,

$$\Omega U_e^{n+1/2} = \sum_j \left[\int_\Omega N_j d\Omega\, U_j^n\right] - \frac{\Delta t}{2}\sum_j\left[\int_\Omega \frac{\partial N_j}{\partial x} d\Omega\, E_j^n + \int_\Omega \frac{\partial N_j}{\partial y} d\Omega\, F_j^n\right] \tag{9}$$

Before advancing the solutions to the second step, the values of U along the outflow boundaries are also required. The following approximations are used for the element boundary of edge S,

$$U^{n+1/2} = U_s^{n+1/2} \tag{10a}$$

$$U^n = \sum_j N_j^s U_j^n \tag{10b}$$

$$E^n = \sum_j N_j^s E_j^n \tag{10c}$$

$$F^n = \sum_j N_j^s F_j^n \tag{10d}$$

where $U_s^{n+1/2}$ denotes the outflow value on the element edge, N_j^s is the interpolation functions along the element edge. The method of weighted residuals is also applied over the edge length, Γ, to yield the equations for computing the element edge quantities,

$$\Gamma U_s^{n+1/2} = \sum_j \left[\int_\Gamma N_j^s\, d\Gamma\, U_j^n\right] - \frac{\Delta t}{2}\sum_j\left[\int_\Gamma \frac{\partial N_j^s}{\partial x} d\Gamma\, E_j^n + \int_\Gamma \frac{\partial N_j^s}{\partial y} d\Gamma\, F_j^n\right] \tag{11}$$

2.2.2) The second step

Using the forward and backward first order Taylor series at time $t = t_{n+1/2}$, the conservation variables at the time t_{n+1} are,

$$U^{n+1} = U^n + \Delta t \left.\frac{\partial U}{\partial t}\right|^{n+1/2} \tag{12}$$

Then substitute Eq. (1) into the right-hand side of Eq. (12) to yield,

$$U^{n+1} = U^n - \Delta t\left[\frac{\partial E}{\partial x}+\frac{\partial F}{\partial y}\right]^{n+1/2} \tag{13}$$

In this second step, the finite element interpolation functions as follows are employed,

$$U^n = \sum_j N_j U_j^n \tag{14a}$$

$$U^{n+1} = \sum_j N_j U_j^{n+1} \tag{14b}$$

$$E^{n+1/2} = E_e^{n+1/2} \quad (14c)$$

$$F^{n+1/2} = F_e^{n+1/2} \quad (14d)$$

where $E_e^{n+1/2}$ and $F_e^{n+1/2}$ are computed directly from $U_e^{n+1/2}$ in Eq. (9). The finite element equations for solving the nodal quantities are obtained by substituting Eq. (14) into Eq. (13) and applying the method of weighted residuals over the element area to yield,

$$\sum_j [M_{ij}(U_j^{n+1} - U_j^n)] = \Delta t \int_\Omega \frac{\partial N_i}{\partial x} d\Omega \, E_e^{n+1/2} \Delta t \int_\Omega \frac{\partial N_i}{\partial y} d\Omega \, F_e^{n+1/2} + R_i^{n+1/2} \quad (15)$$

where $$M_{ij} = \int_\Omega N_i N_j \, d\Omega \quad (16a)$$

$$R_i^{n+1/2} = -\Delta t \int_\Gamma N_i d\Gamma \left[l E_s^{n+1/2} + m F_s^{n+1/2} \right] \quad (16b)$$

In Eq. (16b), l and m are the direction cosines of the outward normal to the surface Γ; $E_s^{n+1/2}$ and $F_s^{n+1/2}$ are the element edge flux vectors along the outflow boundaries and are computed from $U_s^{n+1/2}$ directly. If the values of M_{ij} in Eq. (16a) are diagonalized,

$$M_{ii} = \int_\Omega N_i d\Omega \quad (17)$$

then Eq. (5) can be computed explicitly to yield an explicit algorithm.

This explicit two-step Taylor-Galerkin algorithm is stable under the CFL criterion [9]. The element critical time step, Δt_e, should satisfy,

$$\Delta t_e = \sigma \left[\frac{|\bar{u}|}{\Delta \bar{x}} + \frac{|\bar{v}|}{\Delta \bar{y}} + a \sqrt{\frac{1}{(\Delta \bar{x})^2} + \frac{1}{(\Delta \bar{y})^2}} \right]^{-1} \quad (18)$$

where σ is the Courant number ($0 < \sigma \le 1$), a is the speed of sound, $\bar{u}$ and $\bar{v}$ are the average velocity components of the element, $\bar{x}$ and $\bar{y}$ are the average element sizes in the x and y directions, respectively.

An artificial diffusion is also needed in the algorithm to reduce oscillation of the solutions especially near shock waves. The Lapidus smoothing [10] is selected to contribute artificial diffusion into nodal quantities. These nodal artificial diffusions are determined from,

$$\sum_j [M_{ii}(U_j^{smooth} - U_j^{n+1})] = -\Delta t \left[\int_\Omega \frac{\partial N_i}{\partial x} d\Omega \, \bar{E}_e^{n+1} + \int_\Omega \frac{\partial N_i}{\partial y} d\Omega \, \bar{F}_e^{n+1} \right] \quad (19)$$

where $\bar{E}_e^{n+1}$ and $\bar{F}_e^{n+1}$ are the element artificial flux components in the x and y directions,

$$\bar{E}_e^{n+1} = \lambda \Omega \left| \frac{\partial u}{\partial x} \right| \frac{\partial U}{\partial x} \quad (20a)$$

$$\bar{F}_e^{n+1} = \lambda \Omega \left| \frac{\partial v}{\partial y} \right| \frac{\partial U}{\partial y} \quad (20b)$$

where λ is Lapidus constant ($1 < \lambda < 2$).

3. Examples

Four examples are presented to evaluate the capability of the explicit two-step Taylor-Galerkin algorithm for analysis of high-speed inviscid compressible flows. These four examples are: a Mach 3 flow past a wedge; a Mach 2.6 flow in a channel with compression and expansion ramps; a Mach 6.57 flow past a cylinder; and a Mach 6.57 flow past two cylinders with shock-shock interaction feature. All computations were performed on a standard personal computer with Pentium III 600 MHz processor.

3.1 Mach 3 flow past a wedge

The problem statement of a Mach 3 flow past a wedge is described in Fig. 1(a). The flow enters through the left boundary of the computational domain and creates an oblique shock wave from the compression ramp. The finite element model consisting of 400 triangular elements and 231 nodes, as depicted in Fig. 1 (b), is used in this study. Figure 1(c) shows the predicted density distributions represented by contour lines. The fluid density changes abruptly from the value of one to 2.4 across the oblique shock wave. Because of large element sizes are used, the thickness of the shock wave spreads over approximately two elements. The solution suggests the need of finer mesh, especially along the shock line, to capture the abrupt change of the flow density more accurately.

3.2 Mach 2.6 flow in a channel with compression and expansion ramps

Figure 2(a) shows the problem statement and the sketch of the flow behavior of a Mach 2.6 flow in a reduced channel resulting in a more complex flow field. The flow enters through the left boundary and generates an oblique shock wave from the compression ramp that impinges at the upper wall resulting in a reflecting shock. The mach waves created from the expansion ramp

intersect with the reflecting shock. The finite element model consists of 3,504 triangular elements and 1,850 nodes as shown in Fig. 2(b).

The predicted density distributions represented by contour lines are shown in Fig. 2(c). The two-step Taylor-Galerkin method can provide complex flow behavior from the given finite element mesh. The method generates an oblique shock wave with correct angle from the compression ramp. This shock wave impinges and reflects from the upper wall and is then intersected by the expansion wave from the ramp. The predicted density contours highlight the capability of the explicit two-step Taylor-Galerkin that can capture the complex flow behavior.

3.3 Mach 6.57 flow past a cylinder

A Mach 6.57 flow past a cylinder creating a bow shock is illustrated in Fig. 3(a). Figure 3(b) shows a finite element model consisting of 7,156 triangular elements and 3,727 nodes. Elements are concentrated in front of the cylinder and near the cylinder wall to provide accurate resolution of shock wave and the flow behavior in that region. Figure 3(c) shows the predicted density distributions represented by contour lines. The solution is symmetry for the upper and lower half of the computational domain. This example is used as a basis prior to performing more complex analysis in the next example.

3.4 Mach 6.57 flow past two cylinders with shock-shock interaction phenomenon

To further evaluate the explicit two-step Taylor-Galerkin finite element formulation, the interaction of bow shocks from a Mach 6 flow past two cylinders is performed. The problem statement and the sketch of the flow behavior are shown in Fig. 4(a). The mesh in Fig. 4 (b) consists of 13,805 triangular elements and 7,100 nodes. Small elements are clustered between the two cylinders to capture complex flow behavior in that region.

Figure 4(c) shows the predicted density contours. The figure indicates that bow shock generated from the lower cylinder impinges on the bow shock of the upper cylinder creating a so called Type-IV shock-shock interaction. Such interaction further creates a strong jet that impinges on the upper cylinder surface as enlarged in Fig. 4(d). Figure 4(e) shows the predicted Mach wave distributions that have sharp change across the bow shocks. These figures demonstrate the capability of the explicit two-step Taylor-Galerkin finite element method that can provide detailed flow behavior for high-speed compressible flow past complex geometry.

4. Concluding Remarks

The explicit two-step Taylor-Galerkin algorithm for analysis of two-dimensional inviscid high-speed compressible flow is presented. The finite element equations were derived from the Euler equations and a corresponding computer program that can be executed on standard personal computers has been developed. Four examples of high-speed compressible flow were presented. These examples are: a Mach 3 flow past a wedge; a Mach 2.6 flow in a channel with compression and expansion ramps; a Mach 6.57 flow past a cylinder; and a Mach 6.57 flow past two cylinders with shock-shock interaction phenomenon. The four examples demonstrate that the explicit two-step Taylor-Galerkin algorithm can provide accurate flow solution behavior for high-speed compressible flow analysis.

5. Acknowledgement

The authors are pleased to acknowledge the Thailand Research Fund (TRF), Bangkok, Thailand, for supporting this research work.

References

[1] Anderson, J. D. Jr., Modern Compressible Flow With Historical Prospective, McGraw-Hill, New York, 1982.

[2] Anderson, J. D. Jr., Fundamentals of Aerodynamics, Second Ed., McGraw-Hill, New York, 1991.

[3] Huges, T. J. R., "Recent Progress in the Development and Understanding of SUPG Methods With Special Reference to the Compressible Euler and Navier-Stokes Equations," *International Journal for Numerical Methods in Fluids*, Vol. 7, 1987, pp. 1261-1275.

[4] Jiang, B. N. and Carey, G. F., "A stable Least-Squares Finite Element Method for Non-linear Hyperbolic Problems," *International Journal for Numerical Methods in Fluids*, Vol. 8, 1988, pp. 933-942.

[5] Gnoffo, P. A., "Application of Program LAURA to three-dimensional AOTV Flowfields," AIAA Paper 86-0565, January, 1986.

[6] Dechaumphai, P. and Weiting, A. R., " Coupled Fluid-Thermal-Structural Analysis for Aerodynamically Heated Structures," *Finite Element Analysis in Fluids*, edited by T. J. Chung and G. R. Karr, Univ. Of Alabama in Huntsville Press, Huntsville, AL, April 1989, pp. 165-171.

[7] Dechaumphai, P., Finite Element Method in Engineering, Second Ed., Chulalongkorn University Press, Bangkok, 1999.

[8] Zienkiewicz, O. C., Lohner, R. and Morgan, K., "High Speed Inviscid Compressible Flow by the Finite Element Method," 5th MAFELAP Conference, Brunel University, May, 1984.

[9] Anderson, D. A., Tannehill, J. C. and Pletcher, R. H., Computational Fluid Mechanics and Heat Transfer, New York, John Wiley & Sons, 1995.

[10] Lapidus, A., "A Detached Shock Calculation by Second-Order Finite Differences," *Journal of Computational Physics*, Vol. 2, 1967, pp. 154-177.

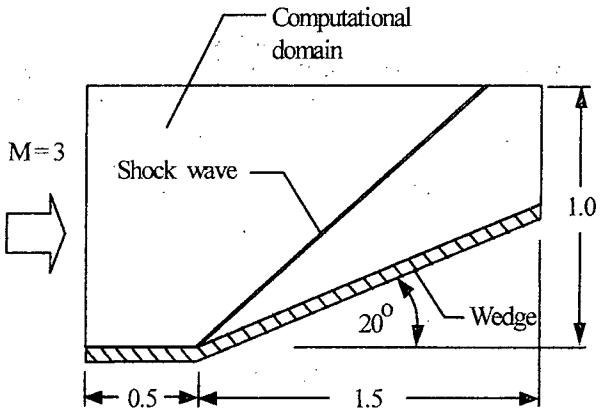

(a) Problem statement.

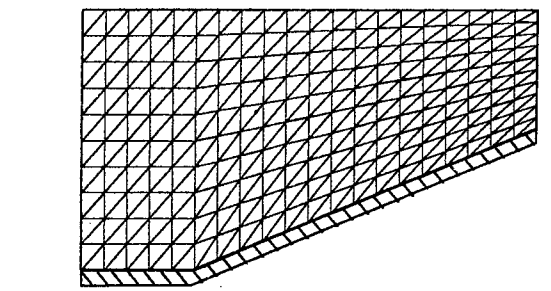

(b) Finite element mesh.

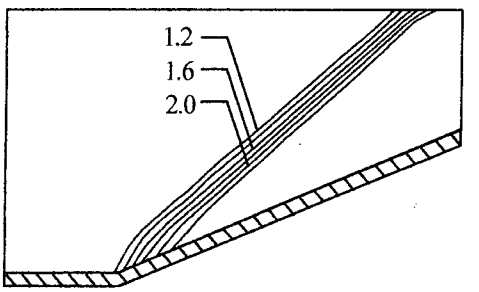

(c) Density contours.

Fig. 1 - Mach 3 flow past a wedge.

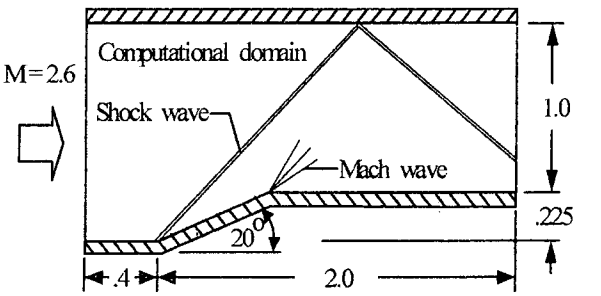

(a) Problem statement.

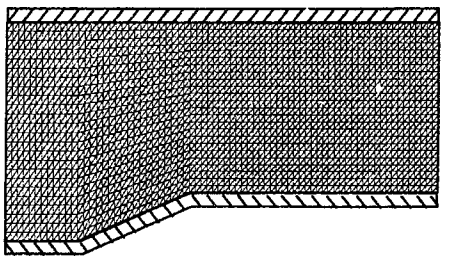

(b) Finite element mesh.

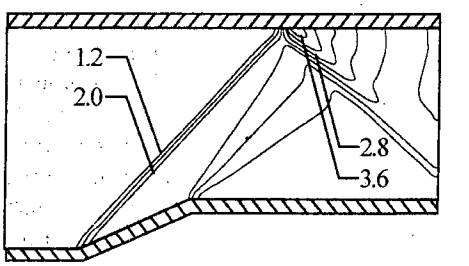

(c) Density contours.

Fig. 2 - Mach 2.6 flow in a channel with compression and expansion ramps.

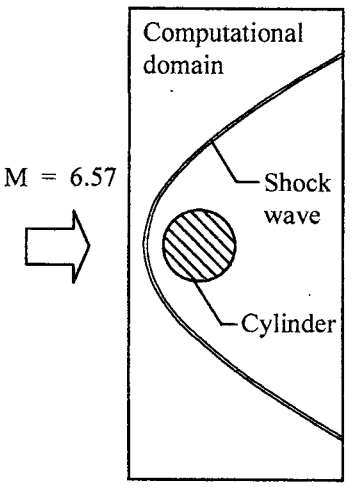

(a) Problem statement.

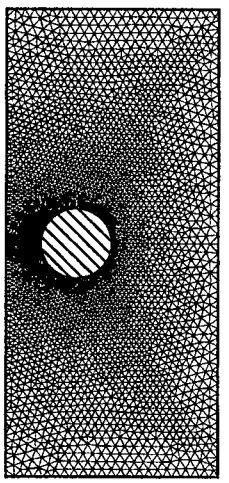

(b) Finite element mesh.

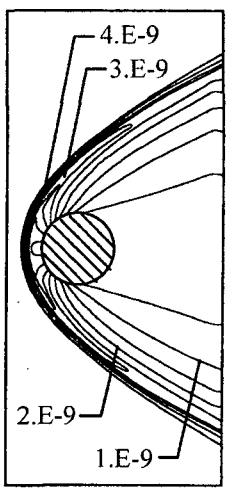

(c) Density contours.

Fig. 3 - Mach 6.57 flow past a cylinder.

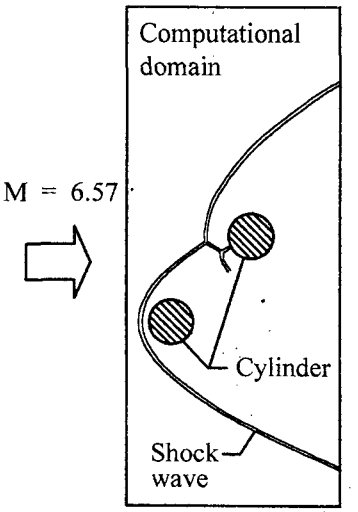

(a) Problem statement.

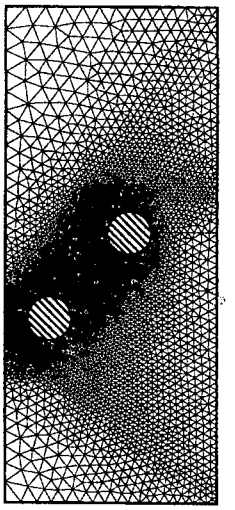

(b) Finite element mesh.

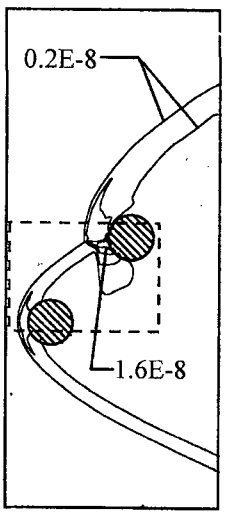

(c) Density contours.

Fig. 4 - Mach 6.57 flow past two cylinders with shock-shock interaction phenomenon.

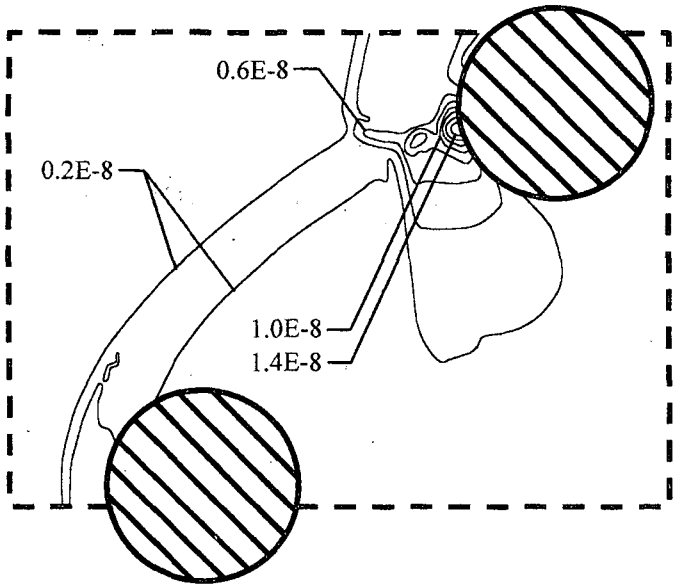

(d) Detailed density distribution.

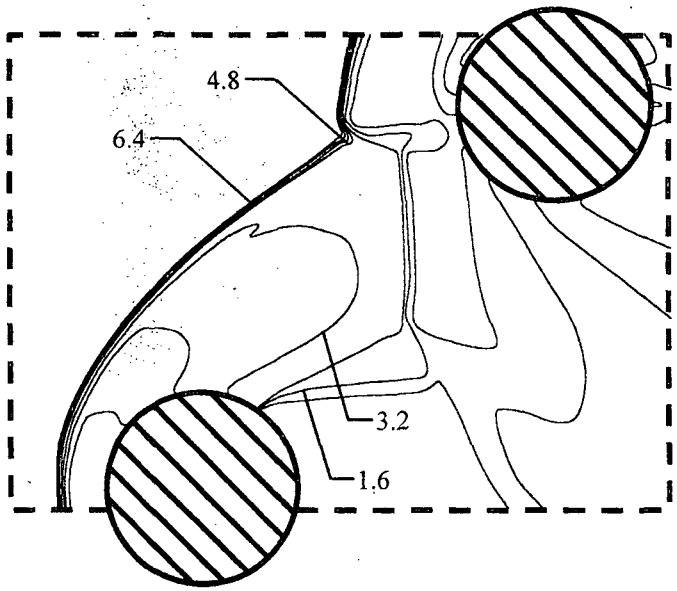

(e) Detailed Mach number distribution.

Fig. 4 (Cont.) - Mach 6.57 flow past two cylinders with shock-shock interaction phenomenon.